MARS GEOLOGY

Carbonates identified by the Curiosity rover indicate a carbon cycle operated on ancient Mars

Benjamin M. Tutolo[1]*, Elisabeth M. Hausrath[2], Edwin S. Kite[3], Elizabeth B. Rampe[4], Thomas F. Bristow[5], Robert T. Downs[6], Allan Treiman[7], Tanya S. Peretyazhko[8], Michael T. Thorpe[9,10,11], John P. Grotzinger[12], Amelie L. Roberts[13], P. Douglas Archer[8], David J. Des Marais[5], David F. Blake[5], David T. Vaniman[14], Shaunna M. Morrison[15,16], Steve Chipera[14], Robert M. Hazen[15], Richard V. Morris[4], Valerie M. Tu[17], Sarah L. Simpson[17], Aditi Pandey[4], Albert Yen[18], Stephen R. Larter[1], Patricia Craig[14], Nicholas Castle[14], Douglas W. Ming[4], Johannes M. Meusburger[5], Abigail A. Fraeman[18], David G. Burtt[10], Heather B. Franz[10], Brad Sutter[8], Joanna V. Clark[17], William Rapin[19], John C. Bridges[20], Matteo Loche[19], Patrick Gasda[21], Jens Frydenvang[22], Ashwin R. Vasavada[18]

Ancient Mars had surface liquid water and a dense carbon dioxide (CO_2)–rich atmosphere. Such an atmosphere would interact with crustal rocks, potentially leaving a mineralogical record of its presence. We analyzed the composition of an 89-meter stratigraphic section of Gale crater, Mars, using data collected by the Curiosity rover. An iron carbonate mineral, siderite, occurs in abundances of 4.8 to 10.5 weight %, colocated with highly water-soluble salts. We infer that the siderite formed in water-limited conditions, driven by water-rock reactions and evaporation. Comparison with orbital data indicates that similar strata (deposited globally) sequestered the equivalent of 2.6 to 36 millibar of atmospheric CO_2. The presence of iron oxyhydroxides in these deposits indicates that a partially closed carbon cycle on ancient Mars returned some previously sequestered CO_2 to the atmosphere.

The geomorphology of Mars demonstrates that the planet formerly hosted large quantities of liquid water on its surface, at least intermittently, which requires a higher temperature than at present (*1*, *2*). Climate models of ancient Mars indicate that to produce sufficiently warm conditions for stable liquid water, the atmosphere must have contained at least tens of millibars of atmospheric carbon dioxide (CO_2) (*1*, *2*) and potentially much more (several bars) (*3*–*5*). The current martian atmosphere contains only ~6 mbar CO_2 (*6*).

It has been estimated that volcanic outgassing would have provided the equivalent of 0.1 to 10 bar of CO_2 to Mars' early atmosphere (*7*, *8*). Much of this CO_2 (up to 3 bar) was subsequently lost to space (*6*), but enough CO_2 must have been present in the atmosphere at some point for liquid water to be stable. Under those conditions, reactions between liquid water and rock (aqueous alteration) are predicted to have produced sedimentary carbonates (*9*, *10*).

There have been several detections of carbonate minerals on Mars (*6*, *11*, *12*), but in lower quantities than were predicted (*10*, *11*, *13*). Carbonates have been identified in situ by using rovers, remotely by orbiters, and in martian meteorites (supplementary text). Those carbonates have a wide range of compositions and mineralogical contexts (*12*) but are mostly iron (Fe)–bearing carbonates with differing (but substantial) magnesium (Mg)–, calcium (Ca)–, and manganese (Mn)–carbonate components (*12*). The chemistry of carbonates can record their formation pathways (*14*, *15*). The measured compositions of martian carbonates are generally consistent with formation through aqueous alteration of basalt, which is supported by their colocation with primary basaltic minerals such as olivine and pyroxene (*12*). These properties have been interpreted as indicating that the dominant mode of carbonate mineral formation on Mars is direct, possibly hydrothermal, replacement of basaltic minerals rather than sedimentary processes (*12*).

Spectroscopic mapping of surface geology from orbit can be used to estimate global mineralogical inventories (*11*). Global deposits of carbonates on Mars are estimated to have sequestered the equivalent of 10 mbar to 1 bar of atmospheric CO_2 (*6*). These estimates span a wide range because few carbonate exposures have been identified from orbit (*16*). Either carbonate minerals are rare on the surface of Mars, or they are present in a form that eludes detection by reflectance and thermal emission spectroscopy. In either case, there is little evidence of the carbonates in sedimentary rocks that are predicted by climate and geochemical models.

Rover drill samples contain siderite

We searched for carbonates using data from the Curiosity rover, part of the Mars Science Laboratory mission, which is exploring Aeolis Mons (informally known as Mount Sharp) in Gale crater, Mars. In late 2022, the rover reached sedimentary strata containing magnesium sulfates (*17*), part of a sulfate-rich unit that had previously been mapped from orbit (*18*). The rover drilled four samples of these rocks (Fig. 1) in locations imaged with the Mast Camera (Mastcam) (*19*). Those samples were analyzed by using the rover's Chemistry and Mineralogy (CheMin) instrument, which uses x-ray diffraction to determine sample mineralogy.

Crystalline starkeyite ($MgSO_4{\cdot}4H_2O$) was present in the drill hole informally called Canaima, which was sampled at –3879 m elevation (relative to Mars mean radius) from the strata informally designated the Contigo member (lithologically distinct subdivision) of a larger sedimentary unit, informally designated the Mirador Formation (*17*). Curiosity then ascended onto a nearby prominent bench informally known as the Marker Band (*20*), which extends almost continuously around Mt. Sharp. Geologically, this is informally designated as the Amapari member of the Mirador Formation. The hard rocks of the wave-rippled strata of the Amapari member could not be drilled, but a drill sample informally named Tapo Caparo was obtained from the overlying thickly laminated strata, at –3853 m elevation (fig. S1) on sol 3752 (where mission sols are martian days elapsed since the rover landed). The Canaima and Tapo Caparo samples were obtained from sedimentary deposits that were laid down in a lacustrine (lakebed) environment. A further drill sample, informally named Ubajara, was acquired at –3826 m elevation on sol 3823, above a transition to sediments from a predominantly eolian (wind-blown) environment (Fig. 1). This unit, informally designated the Chenapau member of the Mirador Formation, has sedimentary features, such as sand sheets (fig. S2), that indicate there was a shallow water table that limited sand accumulation (*21*). Another drill sample, informally named Sequoia, was obtained from Chenapau sandstones at –3764 m elevation on sol 3980 (fig. S3).

[1]Department of Earth, Energy, and Environment, University of Calgary, Calgary, AB, Canada. [2]Department of Geoscience, University of Nevada–Las Vegas, Las Vegas, NV, USA. [3]Department of Geophysical Sciences, University of Chicago, Chicago, IL, USA. [4]Astromaterials Research and Exploration Science Division, NASA Johnson Space Center, Houston, TX, USA. [5]Exobiology Branch, NASA Ames Research Center, Moffett Field, CA, USA. [6]Department of Geosciences, University of Arizona, Tucson, AZ, USA. [7]Lunar and Planetary Institute, Universities Space Research Association, Houston, TX, USA. [8]Amentum, NASA Johnson Space Center, Houston, TX, USA. [9]Department of Astronomy, University of Maryland, College Park, MD, USA. [10]Solar System Exploration Division, NASA Godard Space Flight Center, Greenbelt, MD, USA. [11]Center for Research and Exploration in Space Science and Technology, NASA Goddard Space Flight Center, Greenbelt, MD, USA. [12]Division of Geological and Planetary Sciences, California Institute of Technology, Pasadena, CA, USA, Pasadena, CA, USA. [13]Department of Earth Science and Engineering, Imperial College London, London, UK. [14]Planetary Science Institute, Tucson, AZ, USA. [15]Earth and Planets Laboratory, Carnegie Institution for Science, Washington, DC, USA. [16]Department of Earth and Planetary Sciences, Rutgers University New Brunswick, Piscataway, NJ, USA. [17]Texas State University–Amentum Johnson Space Center Engineering, Technology, and Science II, NASA Johnson Space Center, Houston, TX, USA. [18]Jet Propulsion Laboratory, California Institute of Technology, Pasadena, CA, USA. [19]Institut de Recherche en Astrophysique et Planétologie, Université de Toulouse, CNRS, Centre National d'Études Spatiales, Toulouse, France. [20]Space Park Leicester, University of Leicester, Leicester, UK. [21]Los Alamos National Laboratory, Los Alamos, NM, USA. [22]Globe Institute, University of Copenhagen, Copenhagen K, Denmark.
*Corresponding author. Email: benjamin.tutolo@ucalgary.ca

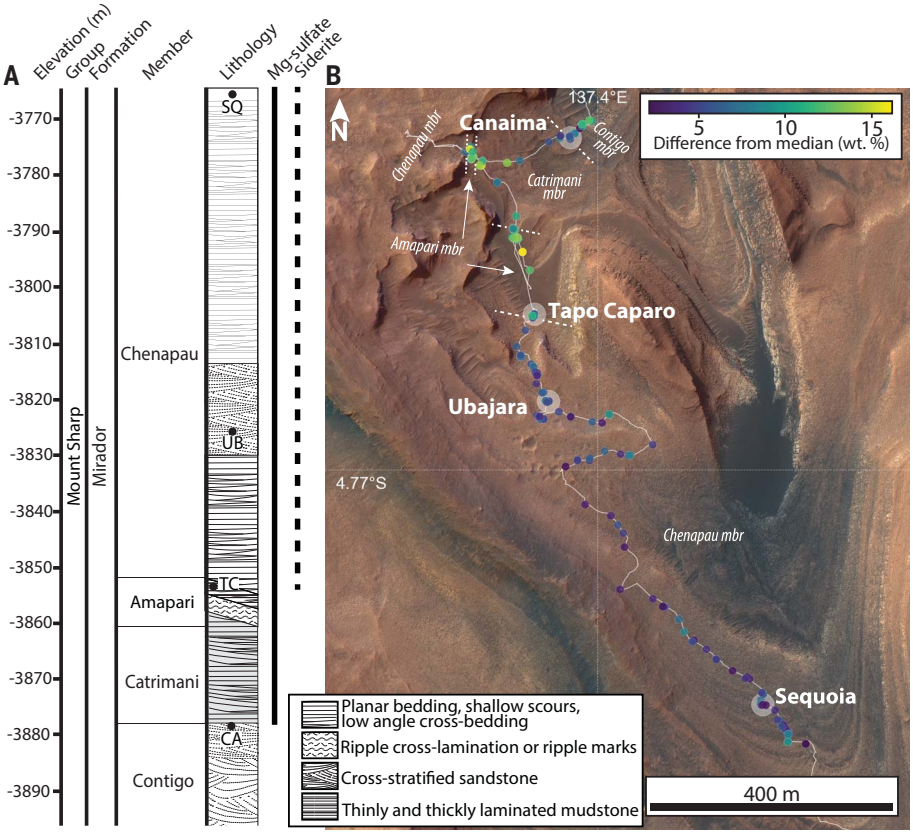

Fig. 1. Geological context of the drill samples. (**A**) Stratigraphic column indicating elevations and sedimentological interpretations of the 89-m vertical section traversed by the rover. Group, formation, and member designate the sedimentary units. Hatching styles indicate the lithology, as indicated in the legend. Black circles indicate drill sample locations: CA, Canaima; TC, Tapo Caparo; UB, Ubajara; and SQ, Sequoia. Vertical thick lines extend between sample elevations where Mg-sulfate minerals (solid line) and siderite (dashed line) have been detected. (**B**) Orbital optical image mosaic of Gale crater, overlain with Curiosity's traverse (white line) up Mt. Sharp. Member (mbr) boundaries correspond to the section in (A). The difference between ChemCam observation points and the median Chenapau bedrock composition (*19*) is plotted as colored circles (as indicated in the color bar) at locations where ChemCam analyses were performed. Chenapau member chemistry is homogeneous and closely resembles the chemistry of the upper section of the Amapari member, near the Canaima drill site.

Table 1. Mineralogical composition of the examined samples. Values of mineral and amorphous component abundance (in weight %) derived from the CheMin data and their 1σ uncertainties. Dashes indicate that the phase was below CheMin detection limit (<1 wt %).

Phase	Tapo Caparo	Ubajara	Sequoia
Plagioclase	15.3 ± 0.7	14.8 ± 1.2	21.1 ± 0.7
Pyroxene	8.7 ± 0.8	6.0 ± 0.8	13.9 ± 0.9
Quartz	–	0.9 ± 0.2	0.9 ± 0.2
Hematite	–	2.3 ± 0.7	2.4 ± 0.7
Goethite	–	1.2 ± 0.2	–
Akageneite	–	–	2.7 ± 0.6
Siderite	10.5 ± 0.5	4.8 ± 0.3	7.6 ± 0.4
Anhydrite	0.8 ± 0.2	0.5 ± 0.2	2.6 ± 0.3
Bassanite	1.5 ± 0.4	0.8 ± 0.1	–
Gypsum	–	2.3 ± 0.2	–
Starkeyite	–	6.4 ± 0.8	–
Kieserite	3.2 ± 0.4	–	5.8 ± 0.8
Amorphous	60 ± 12	60 ± 12	43 ± 13

We analyzed CheMin measurements of each of these four drill samples (figs. S4 to S7) (*19*), finding that the Tapo Caparo, Ubajara, and Sequoia samples contain crystalline siderite ($FeCO_3$) at respective abundances of 10.5 ± 0.5, 4.8 ± 0.3, and 7.6 ± 0.4 wt % (1σ uncertainties). The samples also contain basaltic minerals [the sodium (Na)–, Ca-, and aluminum (Al)–bearing silicate mineral plagioclase and the Ca- and Mg-bearing silicate mineral pyroxene], calcium sulfates, magnesium sulfates, different amounts of iron oxyhydroxides, and an unidentified x-ray amorphous material (Table 1, Fig. 2, and supplementary text). The abundance of siderite in these samples was sufficiently high for our analysis procedure (*19*) to determine the cation compositions of the carbonates (fig. S8). We found that the siderite is highly pure, with estimated formulas of $Fe_{0.97}Mg_{0.03}CO_3$, $Fe_{0.95}Mg_{0.05}CO_3$, and $FeCO_3$ for the Tapo Caparo, Ubajara, and Sequoia siderites, respectively (Fig. 2C).

We confirmed the siderite purity and accompanying mineralogy using the Sample Analysis at Mars (SAM) instrument suite, which combusts samples to produce gases and performs evolved gas analysis (EGA) to determine their chemistry (*19*). EGA of these samples by use of SAM shows that all three exhibit a similar CO_2 release, caused by carbonate mineral thermal decomposition, at temperatures >100°C lower than would be expected from Mg- or Ca-carbonates (fig. S9). The SAM results are consistent with the formulas calculated from the CheMin data for all three samples.

Siderite deposition requires fluid supersaturation

The abundance and composition of the carbonates in the drill samples indicates a sedimentary pathway for carbonate formation and preservation on Mars. Siderite has been theoretically predicted to be a primary, early-forming sedimentary mineral on Mars (*12*, *22*). The nearly pure $FeCO_3$ compositions we found are unlike the Ca- and Mg-rich carbonates that were previously identified in martian samples (Fig. 2C).

The siderite and sulfates in the analyzed sediments were deposited by fluids. We constrained properties of the fluid by considering the mineralogy and geological context of the samples in a geochemical framework (*19*). Like other carbonates (*23*), siderite is much more soluble in an aqueous solution if carbonic acid (H_2CO_3) is more abundant than its dissociation product, bicarbonate (HCO_3^-) (Fig. 3). To allow precipitation, any siderite-forming solution must therefore have substantial alkalinity (effectively, the sum of HCO_3^- and CO_3^{2-} concentration in equivalents units) at neutral or basic pH, depending on the partial pressure of CO_2 (P_{CO_2}) in the solution (Fig. 3). This P_{CO_2} might or might not have been representative of atmospheric P_{CO_2} at the time the siderite

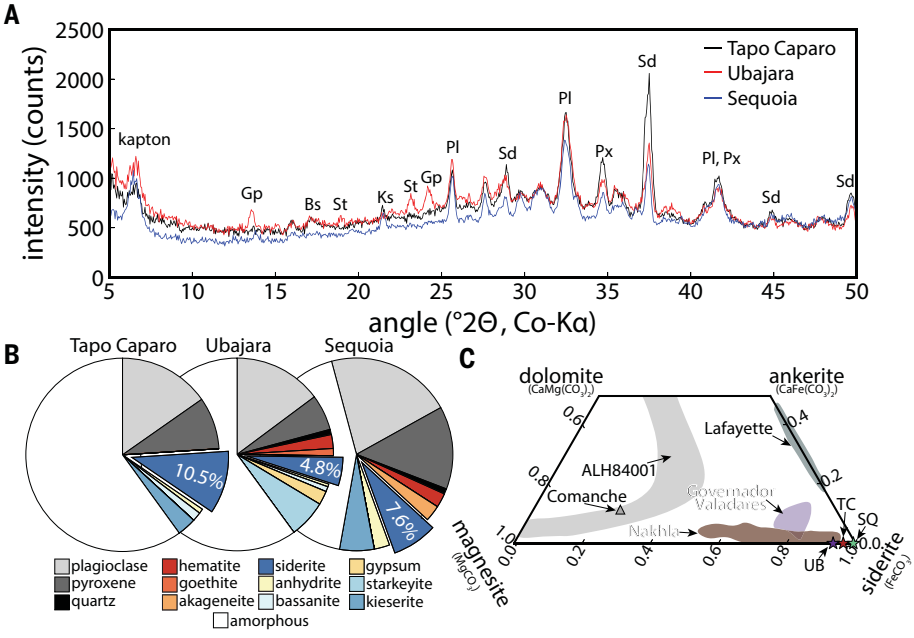

Fig. 2. Mineralogy of the samples and composition of the siderite. (**A**) X-ray diffraction patterns measured with CheMin from three samples (as indicated in the legend). Intensity is plotted as a function of the 2θ diffraction angle, in degrees, corresponding to CheMin's Cobalt (Co) Kα x-ray source (*19*). Peaks are labeled with the identified minerals: Sd, siderite; Gp, gypsum; Px, pyroxene; St, starkeyite; Bs, bassanite; Ks, kieserite; and Pl, plagioclase. A peak due to the Kapton window on the CheMin cell is also labeled. (**B**) Pie charts showing the calculated mineralogical and amorphous phase abundances in the Tapo Caparo, Ubajara, and Sequoia samples. Colors indicate minerals. The siderite wedges are offset and labeled with their abundance. (**C**) The carbonate compositions of the investigated samples (stars, labeled as in Fig. 1A) compared with shaded regions corresponding to the composition of carbonates previously identified in martian meteorites (ALH84001, Lafayette, Nakhla, and Governador Valadares) and at the Comanche outcrop in Gusev Crater (*12*) on a ternary diagram for the Ca, Mg, and Fe carbonate system.

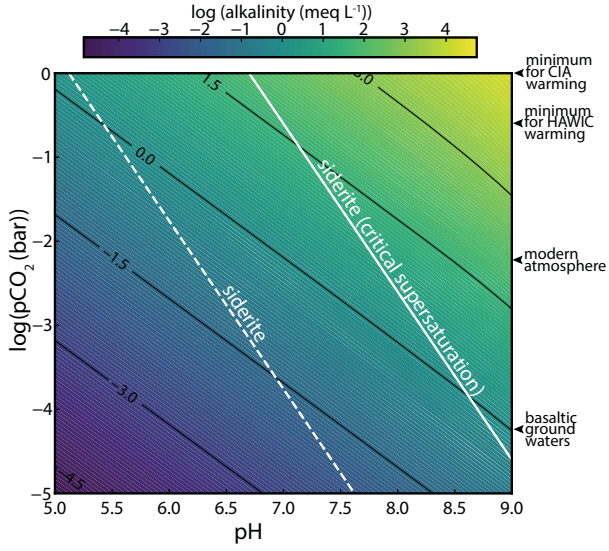

Fig. 3. Thermodynamic requirements for siderite formation. The dashed white line indicates the minimum pH required for siderite precipitation as a function of P_{CO_2}, determined from our thermodynamic solubility calculations (*19*). The thick white line is the same threshold but for the experimentally measured critical supersaturation, which incorporates kinetic inhibition of siderite precipitation (*35*). Color indicates the corresponding alkalinity in milliequivalents per liter (meq L^{-1}); thin black lines are contours labeled with the corresponding values. Black arrowheads indicate the minimum atmospheric P_{CO_2} theoretically predicted to stabilize liquid water in collision-induced absorption (CIA) (*3*) and high-altitude water ice cloud (HAWIC) (*2*) scenarios, and the modern martian atmosphere (*6*). Also indicated is the maximum P_{CO_2} measured in Icelandic basaltic groundwaters (*24*), which is much lower than Earth's atmospheric P_{CO_2} (*19*).

was deposited; less alkalinity is required to precipitate siderite at lower P_{CO_2} typical of basaltic groundwaters (*24*) than at the theoretically predicted P_{CO_2} of the ancient martian atmosphere (Fig. 3). Because siderite contains Fe in its chemically reduced state, the siderite-forming solutions must also have been less oxidized than the modern martian surface and atmosphere, in which the stability of oxidized Fe is demonstrated by the prevalence of oxidized (red) Fe. Isotopic analysis of the siderite shows that it is enriched in heavy isotopes of C and O, relative to both the modern and predicted ancient Mars atmospheres (*25*). Because siderite is preferentially produced in reducing, lower-than-atmospheric P_{CO_2} solutions, we propose that it formed in subsurface pore spaces that were not in direct contact with the atmosphere.

The composition of the siderite provides further constraints on its formation conditions. Because dissolved Mn^{2+} is easily incorporated into siderite (*15*), the lack of measurable Mn^{2+} in the analyzed siderites indicates that the precipitating solution contained little or no Mn^{2+}. Olivines and pyroxenes in martian meteorites usually contain substantial Mn^{2+} (*26*), which would be released alongside Fe^{2+} during basalt dissolution. We therefore infer that the siderite did not form through direct replacement of basaltic minerals. Similarly, the negligible Mg^{2+} contents of the siderite are consistent with formation at low temperature (*14*, *15*). The absence of Ca^{2+} in the siderite indicates a high Fe^{2+}/Ca^{2+} ratio in the precipitating solution at the time of siderite formation (*14*, *15*). The drill samples also contain Ca-sulfate minerals, which require substantial Ca^{2+} and SO_4^{2-} in the solution. We therefore infer that the siderites and sulfates formed from solutions with substantially different Fe^{2+}/Ca^{2+} ratios, or at different times from an evolving solution. This ratio could fall over time if a substantial fraction of Fe was removed through siderite precipitation, leaving Ca still in solution (fig. S10). Sulfates have been prevalent along Curiosity's traverse of Mt. Sharp, and at least some of the sulfates in these drill samples might have formed after the siderite, either through evaporation during early diagenesis (postdepositional changes to the sediment) (*27*) or as veins filling fractures during later diagenesis (*28*, *29*).

Evaporation drove siderite precipitation

Dissolution of basalt could have provided the divalent cations (Fe^{2+}, Ca^{2+}, and Mg^{2+}) required to form the sulfate and carbonate minerals, whereas atmospheric CO_2 and sulfur dioxide (SO_2) could have provided the major anions HCO_3^- and SO_4^{2-}. Even after these solutes were dissolved in the fluid, another mechanism is required to reach sufficient supersaturation for nucleation and growth of the carbonate

and sulfate minerals (or their precursors) to occur. The most straightforward mechanism is evaporation of the water in Gale crater, which is consistent with the stratigraphic transition from shallow lacustrine to shallow water-table eolian deposition (Fig. 1). Gale crater is a closed-basin lake system (*30*, *31*), and other samples collected within the crater contain abundant highly soluble salts that require extensive evaporation for deposition (*9*, *22*, *27*, *32*). Alternative mechanisms to concentrate solutes, such as brine freezeout, could have had a similar overall effect (*22*). Although we cannot eliminate brine freezeout as a potential mechanism, sedimentological criteria (*30*) imply that it is unlikely to have occurred in Gale crater.

We used the concept of chemical divides, which relates sequences of mineral precipitation during evaporation to the chemistry of the evaporating waters (*22*, *33*), to interpret the origin of the sampled mineralogy. Because it is the least soluble, siderite is expected to be the first evaporite mineral to precipitate during evaporation of martian aqueous solutions, except those with highly acidic or sulfate-rich compositions (*9*, *22*). Early siderite formation exhausts the alkalinity, which prevents precipitation of other carbonates such as calcite ($CaCO_3$) or magnesite ($MgCO_3$). Continued evaporation leads to the formation of Ca-sulfate phases, such as anhydrite ($CaSO_4$) or gypsum ($CaSO_4{\cdot}2H_2O$). Further evaporation yields hydrous Mg-sulfates such as kieserite ($MgSO_4{\cdot}H_2O$), epsomite ($MgSO_4{\cdot}7H_2O$), or meridianiite ($MgSO_4{\cdot}11\ H_2O$), depending on temperature (*17*, *22*). Because siderite formation occurs at an earlier stage of evaporative concentration than the precipitation of hydrous Mg-sulfates, the formation of the latter through evaporation of Fe^{2+}-bearing solutions implies an earlier siderite-forming step (*22*). If Fe^{2+} had remained in solution when the Mg-sulfates formed, we expect the simultaneous precipitation of Fe-sulfates such as melanterite ($FeSO_4{\cdot}7H_2O$), which have not been detected (our CheMin data set an upper limit of $\lesssim$1 wt % in the samples) (*22*). The evaporation sequence we expect (fig. S10) is consistent with the measured compositions of the drill samples.

We confirmed the consistent chemical composition of the 89 m of analyzed strata using the Chemistry and Camera (ChemCam) instrument, which uses laser pulses to remotely estimate the chemistry of rocks encountered along the rover's traverse more frequently than is possible by using drill samples (*19*). These analyses demonstrate that the analyzed section of the Mirador Formation is chemically homogeneous and differs from the underlying Mt. Sharp stratigraphy (Fig. 1). This implies that the fluids that deposited carbonate and sulfates were long-lived and affected a substantially thick portion of the Mt. Sharp stratigraphy.

Theoretical models indicate that P_{CO_2} must have been higher on ancient Mars, to stabilize liquid water on the surface long enough to deposit the stratigraphically lower sediments that were previously investigated by Curiosity (*30*). The onset of siderite deposition therefore does not record the beginning of elevated atmospheric P_{CO_2}. Carbonate deposition in Gale crater was likely triggered by a change in the fluid within the crater. We hypothesize that changing global environmental conditions might have decreased water availability and diminished the role of sulfuric acid in mediating geochemical reactions. For identical mineral dissolution rates (for example, under identical pH and temperature), water-rock reactions become more effective at buffering water chemistry under more water-limited conditions because solution chemistry evolves more rapidly as minerals dissolve into smaller solution volumes. Sulfuric acid is thought to be the dominant mediator of water-rock interactions on Mars (*10*). Water-limited reactions would have been more effective at neutralizing acid, particularly if the aqueous solutions were not in direct contact with atmospheric SO_2. Even a low concentration of sulfuric acid in solution lowers the pH sufficiently to inhibit carbonate precipitation (*34*). We calculate (*19*) that siderite precipitation halts (Fig. 3) if solution pH is lower than occurred during sediment deposition in underlying Gale crater sediments [pH 5.2 to 5.6 (*35*)]. We therefore suggest that the appearance of siderite in sediments could mark when sulfuric acid was neutralized by basalt-driven alkalinity generation. Any process that neutralizes sulfuric acid could have led to siderite precipitation (Fig. 3) while also leaching the Mg^{2+} and Ca^{2+} required to trigger sulfate deposition during subsequent evaporation.

Implications for global sulfate-bearing strata

Orbital data have been used to map sulfate-bearing sedimentary strata, similar to those observed in Mt. Sharp, across the planet (*36*). Spectral absorption features associated with carbonate minerals have not been reported in orbital observations of Mt. Sharp's sulfate-bearing strata (*37*). These sulfate-bearing sediments were not expected to be carbonate-bearing. We suggest that the carbonates we identified were invisible to orbital investigation, perhaps owing to dust cover or mixing with other phases, such as Mg-sulfates. Whatever the reason for this discrepancy, if other sulfate deposits on Mars also contain carbonate at similar abundances to those we measured at Gale crater, they might also have eluded detection from orbit.

If the mineralogy of the Mt. Sharp sulfate sediments we investigated is representative of global deposits, they could contain a substantial reservoir of carbon. We considered two scenarios to estimate the amount of CO_2 that these rocks might have sequestered (fig. S11) (*19*). In the first scenario, we assumed that the 89 m of strata investigated by Curiosity represent a brief, carbonate-precipitating interlude and multiplied this thickness by the area of global sulfate strata (*19*). In this case, global sulfate strata contain the equivalent of 2.6 to 5.7 mbar of sequestered CO_2—a similar amount to that contained in the modern martian atmosphere. In the second scenario, we assumed that siderite persists throughout the full volume of global sulfate sediments (*19*). In this case, global sulfate strata could contain the equivalent of 16 to 36 mbar of atmospheric CO_2; the latter value is six times Mars' current atmospheric CO_2 pressure. If that amount of CO_2 was present in the ancient atmosphere, it would have provided sufficient pressure for stable surface liquid water on early Mars because the increased atmospheric pressure suppresses evaporative cooling (*38*, *39*). However, a few tens of millibar of atmospheric CO_2 is inadequate by itself to stabilize liquid water on the early martian surface because it would not provide sufficient warming to raise surface temperatures (*40*–*43*). Because erosion has reduced the size of global sulfate deposits, the values of area and volume used in these calculations are likely to be underestimates (*19*).

Diagenesis returned carbon to the atmosphere

Once formed, siderite can decompose to Fe-oxyhydroxides, releasing CO_2, through changes in environmental parameters, such as pH, P_{CO_2}, redox state, or the flux of ionizing radiation (supplementary text). The differences in Fe-bearing minerals in the otherwise compositionally and geologically (Fig. 1) similar Mg-sulfate–rich Canaima, Tapo Caparo, Ubajara, and Sequoia samples indicates differing degrees of post-depositional siderite destruction and provides a record of an ancient martian carbon cycle, which has not been evident in previously investigated strata (*13*, *27*). The Canaima sample contained no detectable siderite but abundant Fe-oxydydroxides in the form of hematite (α-Fe_2O_3) and goethite (α-FeOOH) (*17*). The Tapo Caparo sample was taken from a location separated from Canaima by the Marker Band, which was impenetrable by Curiosity's drill and therefore perhaps impermeable to water. Tapo Caparo contained abundant siderite and no detectable hematite or goethite. Higher up in the stratigraphy, the Ubajara and Sequoia samples contained less siderite than did the Tapo Caparo sample but abundant hematite with either goethite (in Ubajara) or akageneite (β-FeOOH, in Sequoia) (Table 1). Because these ferric Fe-bearing minerals cannot form from the anoxic solutions that would have precipitated siderite (*44*), their presence indicates that diagenetic transformations caused (at least partial) siderite destruction, Fe-oxyhydroxide formation, and

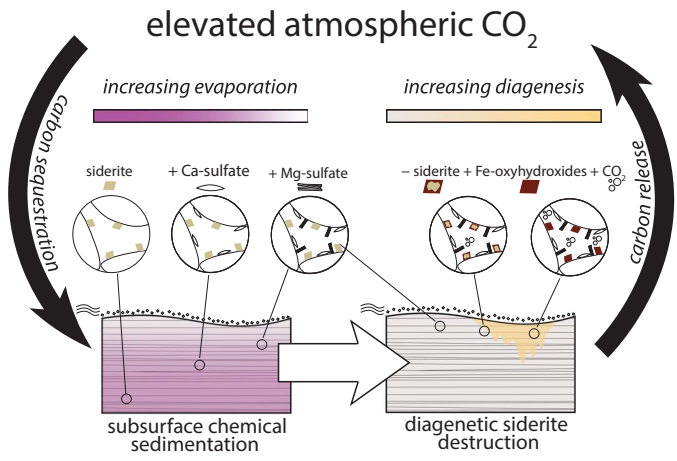

Fig. 4. Schematic illustration of our proposed carbon cycle on early Mars. Evaporation of water (pink shading) from subsurface pore spaces initially deposits siderite, which sequesters atmospheric CO_2 (black downward arrow). Increasing levels of evaporation deposit Ca-sulfate and Mg-sulfate minerals. Wind-blown (eolian) sedimentation at the ground surface (gray dots) moves the location of evaporation and chemical sedimentation upward with time. After some time (white arrow), infiltration of siderite-undersaturated fluids (yellow shading) partially destroys the previously precipitated siderite, forming Fe-oxyhydroxides and releasing previously sequestered CO_2 back into the atmosphere (black upward arrow).

therefore CO_2 release from the Mg-sulfate–bearing strata (Fig. 4). Sulfate-rich, siderite-undersaturated fluids, such as those that formed postdepositional jarosite [$(H_3O^+, K^+, Na^+)Fe_3(SO_4)_2(OH)_6$] in underlying strata (*45*), could have driven this process of carbonate destruction. SAM EGA analyses indicate the presence of Fe-sulfates at abundances below the CheMin detection limit in the investigated samples (fig. S12), which is consistent with this scenario.

Sulfate-bearing formations elsewhere on Mars, mapped by using orbital data, might have experienced a similar sequence of carbonate formation and destruction. Siderite has not been detected in those other deposits, but Fe oxyhydroxides associated with sulfate-bearing strata have been identified in the Valles Marineris and Terra Meridiani formations (*46*). Those oxyhydroxides were hypothesized to have formed from siderite, possibly by acidic groundwaters (*46*). If that interpretation is correct, decomposition of siderite occurred in multiple locations and released CO_2 into the atmosphere, recycling CO_2 that was originally sequestered during siderite formation. Diagenetic carbonate destruction observed elsewhere on Mars (*47*), in martian meteorites (*48*), and in sandstones on Earth (*44*) yields nearly identical reaction products to those we found in Gale crater and are observed globally in orbital data (supplementary text). We therefore conclude that in situ, orbital, and terrestrial analog evidence all indicate that postdepositional alteration of siderite closed the loop in Mars' carbon cycle, by returning CO_2 to the atmosphere (Fig. 4). Yet the persistence of siderite long after deposition indicates that postdepositional siderite destruction was incomplete, and more carbon was sequestered than was subsequently released. The ancient martian carbon cycle was thus imbalanced, in contrast with Earth's, which has remained balanced over geologic time (*49*).

REFERENCES AND NOTES

1. E. S. Kite, L. J. Steele, M. A. Mischna, M. I. Richardson, *Proc. Natl. Acad. Sci. U.S.A.* **118**, e2101959118 (2021).
2. R. A. Urata, O. B. Toon, *Icarus* **226**, 229–250 (2013).
3. R. Wordsworth *et al.*, *Nat. Geosci.* **14**, 127–132 (2021).
4. R. M. Ramirez *et al.*, *Nat. Geosci.* **7**, 59–63 (2014).
5. R. Wordsworth *et al.*, *Geophys. Res. Lett.* **44**, 665–671 (2017).
6. B. M. Jakosky, *Planet. Space Sci.* **175**, 52–59 (2019).
7. B. D. Stanley, M. M. Hirschmann, A. C. Withers, *Geochim. Cosmochim. Acta* **75**, 5987–6003 (2011).
8. H. Lammer *et al.*, *Space Sci. Rev.* **174**, 113–154 (2013).
9. D. C. Catling, *J. Geophys. Res.* **104** (E7), 16453–16469 (1999).
10. S. M. McLennan, J. P. Grotzinger, J. A. Hurowitz, N. J. Tosca, *Annu. Rev. Earth Planet. Sci.* **47**, 91–118 (2019).
11. B. L. Ehlmann, C. S. Edwards, *Annu. Rev. Earth Planet. Sci.* **42**, 291–315 (2014).
12. J. C. Bridges, L. J. Hicks, A. H. Treiman, in *Volatiles in the Martian Crust*, J. Filiberto, S. P. Schwenzer, Eds. (Elsevier, 2019), pp. 89–118.
13. T. F. Bristow *et al.*, *Proc. Natl. Acad. Sci. U.S.A.* **114**, 2166–2170 (2017).
14. C. S. Romanek *et al.*, *Geochim. Cosmochim. Acta* **73**, 5361–5376 (2009).
15. R. Sengupta, N. J. Tosca, S. A. Robinson, *Geochim. Cosmochim. Acta* **271**, 1–15 (2020).
16. C. S. Edwards, B. L. Ehlmann, *Geology* **43**, 863–866 (2015).
17. S. J. Chipera *et al.*, *J. Geophys. Res. Planets* **128**, e2023JE008041 (2023).
18. R. Anderson, J. F. I. Bell, *Mars* **5**, 76–128 (2010).
19. Materials and methods are available as supplementary materials.
20. C. M. Weitz *et al.*, *J. Geophys. Res. Planets* **127**, e2022JE007211 (2022).
21. G. Kocurek, J. Nielson, *Sedimentology* **33**, 795–816 (1986).
22. N. J. Tosca, S. M. McLennan, *Earth Planet. Sci. Lett.* **241**, 21–31 (2006).
23. B. M. Tutolo, A. Awolayo, C. Brown, *Environ. Sci. Technol.* **55**, 11906–11915 (2021).
24. S. Arnorsson, I. Gunnarsson, A. Stefansson, A. Andresdottir, A. E. Sveinbjörnsdóttir, *Geochim. Cosmochim. Acta* **66**, 4015–4046 (2002).
25. D. G. Burtt *et al.*, *Proc. Natl. Acad. Sci. U.S.A.* **121**, e2321342121 (2024).
26. J. J. Papike, J. M. Karner, C. K. Shearer, P. V. Burger, *Geochim. Cosmochim. Acta* **73**, 7443–7485 (2009).
27. W. Rapin *et al.*, *Nat. Geosci.* **12**, 889–895 (2019).
28. M. Nachon *et al.*, *J. Geophys. Res. Planets* **119**, 1991–2016 (2014).
29. J. L'Haridon *et al.*, *Icarus* **311**, 69–86 (2018).
30. J. P. Grotzinger *et al.*, *Science* **350**, aac7575 (2015).
31. W. Rapin *et al.*, *Geology* **49**, 842–846 (2021).
32. J. A. Berger *et al.*, *J. Geophys. Res. Planets* **125**, e2020JE006536 (2020).
33. H. P. Eugster, L. A. Hardie, "Saline Lakes" in *Lakes: Chemistry, Geology, Physics*, A. Lerman, Ed. (Springer, 1978), pp. 237–293.
34. A. G. Fairén, D. Fernández-Remolar, J. M. Dohm, V. R. Baker, R. Amils, *Nature* **431**, 423–426 (2004).
35. N. J. Tosca, I. A. M. Ahmed, B. M. Tutolo, A. Ashpitel, J. A. Hurowitz, *Nat. Geosci.* **11**, 635–639 (2018).
36. J. P. Grotzinger, R. E. Milliken, in *Sedimentary Geology of Mars*, SEPM Special Publications, vol. 102, J. R. Grotzinger, R. E. Milliken, Eds. (SEPM Society for Sedimentary Geology, 2012), pp. 1–48.
37. A. A. Fraeman *et al.*, *J. Geophys. Res. Planets* **121**, 1713–1736 (2016).
38. A. P. Ingersoll, *Science* **168**, 972–973 (1970).
39. M. H. Hecht, *Icarus* **156**, 373–386 (2002).
40. S. W. Squyres, J. F. Kasting, *Science* **265**, 744–749 (1994).
41. R. Wordsworth *et al.*, *Icarus* **222**, 1–19 (2013).
42. M. Turbet, H. Tran, *J. Geophys. Res. Planets* **122**, 2362–2365 (2017).
43. E. S. Kite *et al.*, *Sci. Adv.* **8**, eabo5894 (2022).
44. H. Yoshida *et al.*, *Sci. Adv.* **4**, eaau0872 (2018).
45. P. E. Martin *et al.*, *J. Geophys. Res. Planets* **122**, 2803–2818 (2017).
46. J. P. Bibring *et al.*, *Science* **317**, 1206–1210 (2007).
47. J. Carter, C. Viviano-Beck, D. Loizeau, J. Bishop, L. Le Deit, *Icarus* **253**, 296–310 (2015).
48. J. D. Piercy, J. C. Bridges, L. J. Hicks, *Geochim. Cosmochim. Acta* **326**, 97–118 (2022).
49. C. T. A. Lee, H. Jiang, R. Dasgupta, M. Torres, in *Deep Carbon: Past to Present*, B. N. Orcutt, I. Daniel, R. Dasgupta, Eds. (Cambridge Univ. Press, 2019), pp. 313–357.
50. T. Bristow, B. M. Tutolo, Data from: In situ evidence of an active carbon cycle on ancient Mars. *Astrobiology Habitable Environment Database* (2024); https://doi.org/10.48667/tvxy-6a39.

ACKNOWLEDGMENTS

Mastcam mosaics were processed by the Mastcam team at Malin Space Science Systems. We thank J. Sneed and D. P. Mayer for help in calculating global stratum volumes. We acknowledge the support of the Jet Propulsion Laboratory engineering and management teams and Mars Science Laboratory science team members who participated in tactical and strategic operations, without whom the data presented here could not have been collected. **Funding:** B.M.T. acknowledges funding from the Canadian Space Agency, grant 22EXPMSLCA. E.M.H., E.S.K., and M.T.T. acknowledge funding from NASA grants 80NSSC22K0656 (E.M.H.), 80NSSC22K0731 (E.S.K.), and 80GSFC21M0002 (M.T.T.). T.F.B. acknowledges support for CheMin operations provided by NASA's Mars Exploration Program. A.L.R. acknowledges funding from the Science and Technology Funding Council of the United Kingdom, grant ST/W507520/1. J.C.B. acknowledges funding from the UK Space Agency. P.G. acknowledges support for ChemCam activities from the NASA Mars Exploration Program, grant R-00727-24-0.2. A portion of this research was carried out by A.Y., A.A.F., and A.R.V. at the Jet Propulsion Laboratory, California Institute of Technology, under a contract with NASA (80NM0018D0004). **Author contributions:** B.M.T. wrote the manuscript. B.M.T., E.M.H., E.B.R., T.F.B., R.T.D., A.T., T.S.P., M.T.T., D.J.D.M., D.F.B., D.T.V., S.M.M., S.C., R.M.H., R.V.M., V.M.T., S.L.S., A.P., A.Y., P.C., N.C., D.W.M., and J.M.M. processed, analyzed, and interpreted the CheMin data. P.D.A., D.G.B., H.B.F., B.S., and J.V.C. led the interpretation of the SAM data. A.L.R. and J.P.G. led the stratigraphic interpretation. J.F. led the ChemCam data interpretation. J.C.B., A.T., R.V.M., D.W.M., W.R., and H.B.F. assisted with comparisons to prior martian carbonate identifications. A.A.F. led the analysis and interpretation of orbital data. B.M.T., E.M.H., A.T., D.G.B., T.S.P., S.R.L., W.R., M.L., and P.G. interpreted geochemical pathways to the observed mineralogical assemblages. E.S.K. led the sulfate volume and area calculations and discussed the implications for Mars atmospheric evolution. A.R.V. managed the project and guided the mission. All coauthors commented on the results and revised the text. **Competing interests:** The authors declare that they have no competing interests. **Data and materials availability:** The Curiosity data are archived in NASA's Planetary Data System (PDS).

The MastCam images used to produce the drill site mosaics are available from PDS at https://planetarydata.jpl.nasa.gov/img/data/msl/msl_mmm/data_MSLMST. Text lists (.lst) of the constituent images that compose the mosaics are provided at the Astrobiology Habitable Environment Database (AHED) repository (*50*). The ChemCam spectra are available from PDS at https://pds-geosciences.wustl.edu/msl/msl-m-chemcam-libs-4_5-rdr-v1/mslccm_1xxx/data. Information for extracting the specific spectra used (target name, sol, spacecraft clock identifications), details about analysis locations, and the calculated Euclidian distances are included in the AHED repository (*51*). The CheMin diffraction data were level 4 data products archived in PDS at https://pds-geosciences.wustl.edu/msl/msl-m-chemin-4-rdr-v1/mslcmn_1xxx/data/rdr4. We used the .lbl and .csv files containing (in their file names) the following values of the spacecraft clock: Tapo Caparo 730910626, Ubajara 737119969, and Sequoia 751061408. The derived mineral abundances are level 5 data products archived in PDS at https://pds-geosciences.wustl.edu/msl/msl-m-chemin-4-rdr-v1/mslcmn_1xxx/data/rdr5, with the corresponding spacecraft clock identifications. These data are also archived in the Gale crater Mineralogy and Geochemistry database at https://odr.io/CheMin#/search/display/84/eyJkdF9pZCI6IjQzIn0/1. The SAM EGA data are available in PDS at https://pds-geosciences.wustl.edu/msl/msl-m-sam-2-rdr-l0-v1/mslsam_1xxx/data. We used the level 1b data for samples eid25719 (Tapo Caparo 1), eid25723 (Tapo Caparo 2), eid25729 (Ubajara), eid25743 (Sequoia 1), and eid25746 (Sequoia 2). The modified FULLPAT software used in our CheMin data analysis, the code we used to calculate siderite chemical formulas, and the code we used to calculate sulfate strata volume are archived in the AHED repository (*50*).

SUPPLEMENTARY MATERIALS

science.org/doi/10.1126/science.ado9966
Materials and Methods
Supplementary Text
Figs. S1 to 12
Table S1
References (*51*–*122*)
Data S1 and S2

Submitted 1 March 2024; accepted 25 February 2025
10.1126/science.ado9966